Caspase-1 inhibition prevents glial inflammasome activation and pyroptosis in models of multiple sclerosis

Brienne A. McKenzie[a], Manmeet K. Mamik[b], Leina B. Saito[a], Roobina Boghozian[b,c], Maria Chiara Monaco[d], Eugene O. Major[d], Jian-Qiang Lu[e,f], William G. Branton[b], and Christopher Power[a,b,f,1]

[a]Department of Medical Microbiology and Immunology, University of Alberta, Edmonton, AB T6G 2R3, Canada; [b]Division of Neurology, Department of Medicine, University of Alberta, Edmonton, AB T6G 2R3, Canada; [c]Department of Immunology, Tehran University of Medical Sciences, Tehran 1417653761, Iran; [d]National Institute of Neurological Disorders and Stroke, National Institutes of Health, Bethesda, MD 20892; [e]Department of Laboratory Medicine and Pathology, University of Alberta, Edmonton, AB T6G 2R3, Canada; and [f]Neuroscience and Mental Health Institute, University of Alberta, Edmonton, AB T6G 2R3, Canada

Edited by Lawrence Steinman, Stanford University School of Medicine, Stanford, CA, and approved April 30, 2018 (received for review December 20, 2017)

Multiple sclerosis (MS) is a progressive inflammatory demyelinating disease of the CNS of unknown cause that remains incurable. Inflammasome-associated caspases mediate the maturation and release of the proinflammatory cytokines IL-1β and IL-18 and activate the pore-forming protein gasdermin D (GSDMD). Inflammatory programmed cell death, pyroptosis, was recently shown to be mediated by GSDMD. Here, we report molecular evidence for GSDMD-mediated inflammasome activation and pyroptosis in both myeloid cells (macrophages/microglia) and, unexpectedly, in myelin-forming oligodendrocytes (ODCs) in the CNS of patients with MS and in the MS animal model, experimental autoimmune encephalomyelitis (EAE). We observed inflammasome activation and pyroptosis in human microglia and ODCs in vitro after exposure to inflammatory stimuli and demonstrate caspase-1 inhibition by the small-molecule inhibitor VX-765 in both cell types. GSDMD inhibition by siRNA transduction suppressed pyroptosis in human microglia. VX-765 treatment of EAE animals reduced the expression of inflammasome- and pyroptosis-associated proteins in the CNS, prevented axonal injury, and improved neurobehavioral performance. Thus, GSDMD-mediated pyroptosis in select glia cells is a previously unrecognized mechanism of inflammatory demyelination and represents a unique therapeutic opportunity for mitigating the disease process in MS and other CNS inflammatory diseases.

pyroptosis | gasdermin D | multiple sclerosis | EAE | inflammasome

Inflammasomes are cytosolic protein complexes that are pivotal mediators of innate immunity, particularly in myeloid cells (1). Inflammasome activation is initiated by binding of cytoplasmic sensor proteins to microbial-associated molecular patterns or damage-associated molecular patterns (DAMPs) produced by stressed or dying host cells (e.g., ATP) (2). Certain cytokines, including TNFα, can also drive inflammasome activation (3). A multitude of inflammasome-associated sensor proteins have been identified, including NLRP3 (which detects diverse DAMPs), AIM2 (which detects double-stranded cytoplasmic DNA), NLRP1 (which detects bacterial toxins), and pyrin (which detects modified Rho-GTPases) (4). Oligomerization of sensor proteins with the scaffolding protein ASC and proinflammatory caspases (caspase-1 and -4/5 in humans and caspase-1 and -11 in mice) generates the inflammasome complex; this facilitates caspase autoactivation and the subsequent proteolytic cleavage and release of IL-1β and IL-18. These cytokines induce local inflammation through the NF-κB, AP1, and JNK pathways (2, 5, 6).

Activation of proinflammatory caspases can also drive pyroptosis ("fiery death"), a type of proinflammatory programmed cell death mediated by gasdermin D (GSDMD) [reviewed in ref. 7]. Constitutively expressed GSDMD is retained in a state of autoinhibition mediated by the C terminus of the protein, which is released upon cleavage by proinflammatory caspases (8). Activated GSDMD translocates to the plasma membrane, binds to inner membrane lipids, and oligomerizes to form membrane pores, which cause localized cellular swelling (pyroptotic bodies), membrane rupture, and extravasation of cellular contents (7, 9–11).

Inflammasome activation and pyroptosis have been reported in multiple cell types of the CNS (12). Human microglia, neurons, and astrocytes all display robust NRLP3 inflammasome-associated responses (12). Neurons also express NLRP1 and AIM2 (13), while astrocytes express NLRC4 and NLRP2 (14, 15). However, neither inflammasome activation nor pyroptosis has been investigated in myelin-forming oligodendrocytes (ODCs).

Although low-level IL-1β and IL-18 are required for healthy CNS function, and cytokine deficiencies result in adverse outcomes (16), prolonged elevation of these cytokines causes neurotoxicity (17, 18). Both IL-1β and IL-18 also trigger secondary inflammatory cascades in the CNS, perpetuating neuroinflammation and the release of neurotoxic inflammatory mediators (19). Inflammasomes have been implicated in the pathogenesis of multiple CNS diseases, including Alzheimer's disease, traumatic brain/spinal cord injury, and epilepsy (12, 20). Although pyroptosis has been proposed in several

Significance

The pore-forming protein gasdermin D (GSDMD) was recently identified as the principal executioner of pyroptosis ("fiery death"), a type of proinflammatory programmed cell death driven by inflammasomes. Caspase-1 cleaves GSDMD, but whether this process contributes to neuroinflammation is unknown. Here, we report evidence of GSDMD-mediated pyroptosis as a primary mechanism of inflammatory demyelination in the central nervous system during multiple sclerosis (MS), a debilitating and incurable demyelinating disease that causes profound loss of myelin-forming oligodendrocytes. By identifying GSDMD induction and pyroptosis in oligodendrocytes and microglia, we discovered a previously unrecognized mechanism driving neuroinflammation and demyelination. Pharmacologically inhibiting caspase-1 prevented pyroptosis in experimental models of MS, reducing demyelination and neurodegeneration. These findings highlight therapeutic approaches for understanding and treating inflammatory demyelination.

Author contributions: B.A.M. and C.P. designed research; B.A.M., M.K.M., L.B.S., R.B., J.-Q.L., W.G.B., and C.P. performed research; M.C.M. and E.O.M. contributed new reagents/analytic tools; B.A.M., M.K.M., L.B.S., and W.G.B. analyzed data; J.-Q.L. performed pathology; and B.A.M. and C.P. wrote the paper.

The authors declare no conflict of interest.

This article is a PNAS Direct Submission.

[1]To whom correspondence should be addressed. Email: chris.power@ualberta.ca.

This article contains supporting information online at www.pnas.org/lookup/suppl/doi:10.1073/pnas.1722041115/-/DCSupplemental.

Published online June 12, 2018.

of these disorders, the role of GSDMD in the CNS has not yet been examined.

Multiple sclerosis (MS) is an incurable and progressive CNS disease that affects over 2.5 million people globally and causes motor, sensory, visual, cognitive, autonomic, and mood impairment (21). While the etiology of MS is uncertain, its neuropathological features include inflammatory demyelination, neurodegeneration, and axonal transection/loss (22). Infiltrating lymphocytes in the CNS are less apparent as MS progresses, while microglial and astrocyte activation persists as the defining feature of lesions in progressive MS (23). Indeed, myeloid cell infiltration and activation are key features of contemporary MS lesion categorization (24).

Multiple lines of evidence point to an important role for inflammasomes in MS and its prototypic animal model, experimental autoimmune encephalomyelitis (EAE). Multiple inflammasome-associated proteins, including caspase-1, ASC, NLRP3, IL-18, and IL-1β, are expressed in MS lesions (reviewed in refs. 25–27). Of interest, the cryopyrin-associated periodic syndromes, inflammatory disorders caused by gain-of-function mutations in the *NLRP3* gene, can present with neurological manifestations and MS-like lesions (28–30). In EAE, deletion of inflammasome genes (e.g., ASC$^{-/-}$ and caspase-1$^{-/-}$) (31) reduces the severity of disease, while NLRP3$^{-/-}$ mice display variable outcomes (31, 32). IL-1β itself has been shown to increase the permeability of the blood–brain barrier, facilitate leukocyte infiltration, and promote neurotoxicity in the EAE model (reviewed in ref. 25). Pharmacological inhibition of NLRP3 or the upstream P2X7 receptor also attenuates EAE disease severity (33, 34). Of note, inflammasomes are regulated by type 1 IFNs, but IFN-β exerts variable effects on EAE-induced inflammasome activation, depending on the specific EAE induction conditions (35, 36). Most genetic and therapeutic intervention studies in EAE have focused on the effects of inflammasome activation in circulating leukocytes, particularly on T cell priming and infiltration into the CNS (37–39). However, inflammasome activation and pyroptosis in the CNS remain poorly defined.

We hypothesized that CNS inflammasome activation and GSDMD-mediated pyroptosis occur in MS and EAE, driving pathogenesis and neurological disability. The objectives of the present study were to define an inflammasome signature within the CNS for MS and EAE, to evaluate the molecular and morphological evidence for CNS GSDMD expression and pyroptosis, and to define the impact of CNS inflammasome regulation through caspase-1 inhibition.

Results

CNS Inflammasome Activation and Pyroptosis in MS. Earlier studies have reported increased expression of inflammasome components in CNS tissues from patients with MS (40, 41). To examine CNS inflammasome expression in a systematic manner, a wider panel of inflammasome genes was assessed in postmortem samples from the frontal white matter of age- and sex-matched MS and non-MS patients (*SI Appendix*, Table S1). Transcript was detectable for all inflammasome-associated genes examined in human CNS tissue, with increased *IL1B*, *IL18*, *CASP1*, and *GSDMD* transcript levels in MS compared with non-MS samples (Fig. 1*A*). Similarly, transcripts were detectable for all inflammasome sensors examined, including *MEFV* (encoding pyrin), *NLRP3*, *NLRP1*, *AIM2*, and *NLRP2* in MS tissue. *NLRP3* expression was significantly elevated in MS white matter compared with non-MS controls (Fig. 1*B*). *AIM2* levels were significantly elevated when all patients were included in the dataset; however, upon exclusion of the highest outlier, *AIM2* transcript levels in MS patients only trended upwards compared with non-MS controls ($P = 0.059$ with outlier excluded versus $P = 0.0365$ with outlier included).

These findings prompted further examination of inflammasome-associated proteins in the CNS. Comparison of non-MS white matter with MS lesions revealed increased MHC class II immunoreactivity at the border of a demyelinated lesion (Fig. 1 *C*, *ii*), indicating the robust recruitment of activated antigen-presenting cells in MS white matter, which was not observed in non-MS tissue (Fig. 1 *C*, *i*). IL-1β immunoreactivity was negligible in non-MS white matter (Fig. 1 *D*, *i*), while IL-1β immunopositive cells were observed in MS tissues (Fig. 1 *D*, *ii*). Immunofluorescent labeling demonstrated IL-1β immunoreactivity in MHC II$^+$ myeloid cells (*SI Appendix*, Fig. S1*B*). Caspase-1 immunoreactivity was detected in occasional cells in the white matter of non-MS tissue (Fig. 1 *E*, *i*) but was markedly increased in MS tissues (Fig. 1 *E*, *ii*) and localized within MHC II$^+$ cells around blood vessels and in the CNS parenchyma (*SI Appendix*, Fig. S1*A*). Although limited GSDMD immunoreactivity was observed in non-MS white matter (Fig. 1 *F*, *i*), intense GSDMD immunostaining concentrated at the plasma membrane was observed in MS white matter (Fig. 1 *F*, *ii*, *Inset*), forming a "ring of fire" that is consistent with GSDMD's role as a pore-forming membrane protein during pyroptosis. Quantification of the frequency of immunopositive cells verified a robust increase ($P < 0.0001$) in the number of IL-1β$^+$, caspase-1$^+$, and GSDMD$^+$ cells in white matter of MS versus non-MS patients (Fig. 1*I*).

In active MS lesions, cellular debris that was DAPI stained and GSDMD immunopositive was observed (Fig. 1*G*), with only a few remaining intact nuclei, potentially indicating widespread death of GSDMD$^+$ cells. Among the intact cells, GSDMD immunolabeling was often expressed within Iba-1$^+$ cells (Fig. 1*G*, *Insets*). Unexpectedly, GSDMD was also detected in GST-pi$^+$ ODCs (Fig. 1*H*, *Insets*: GSDMD, red; GST-pi, green; DAPI, blue; overlap appears yellow), both with intact (Fig. 1*H*) and dysmorphic (*SI Appendix*, Fig. S1*C*) nuclei. To quantify coexpression of GSDMD with these cell markers of interest, the proportion of microglia (Iba-1$^+$) and ODCs (GST-pi$^+$) that were GSDMD$^+$ was calculated in a subset of patients (Fig. 1*J*). The proportion of GSDMD$^+$ Iba-1$^+$ microglia in MS white matter (46%) was higher than the proportion (24%) in non-MS samples ($P < 0.0001$). This was recapitulated in the GST-pi$^+$ ODCs, wherein 53% of ODCs in MS white matter expressed GSDMD, compared with 38% in non-MS controls ($P < 0.0001$). The robust increase in the proportion of microglia and ODCs expressing GSDMD underscored the potential impact of inflammasome activation and pyroptosis on MS pathogenesis.

Inflammasome Activation and Pyroptosis in Human Microglia. To verify the above findings, inflammasome activation and pyroptosis in response to MS-relevant stimuli were assessed in both cultured human microglia and ODCs. The caspase-1 inhibitor VX-765 was tested in both cell types to assess its efficacy for later use in vivo.

First, microglia were exposed to the NLRP3 inflammasome activator nigericin with or without the caspase-1 inhibitor VX-765 (Fig. 2) (42). Nigericin was selected for initial VX-765 validation purposes due to its significant and reproducible induction of both inflammasome activation and pyroptosis (43). Additionally, nigericin is a specific inducer of the NLRP3 inflammasome, the major sensor for DAMPs upstream of inflammasome activation; since NLRP3 emerged in MS as an inflammasome of interest (Fig. 1), an NLRP3-specific, well-characterized inflammasome activator was initially used for validating VX-765 ex vivo.

Using confocal microscopy, we characterized the process of microglial pyroptosis following nigericin exposure (4 h, 5 μM). The human microglia utilized for these experiments expressed microglial markers including Iba-1 constitutively (*SI Appendix*, Fig. S2*A*), which was not significantly affected by nigericin exposure (*SI Appendix*, Fig. S2 *B* and *D*). Nigericin-exposed microglia demonstrated a distinctive pyroptotic phenotype (Fig. 2*B*), including the ring of fire, defined by a rounded morphology and the localization of GSDMD to the plasma membrane, often within pyroptotic bodies (Fig. 2 *B*, *i*, arrows). Microglia at this stage of pyroptosis (*SI Appendix*, Fig. S3) had an average of 7.2 ± 1.7 pyroptotic bodies per cell, averaging 8.2 ± 0.9 μm^2. Furthermore, the ratio of GSDMD immunoreactivity in pyroptotic bodies compared with the cytoplasm was higher in microglia undergoing pyroptosis than in control cells, which had occasional membrane protrusions ($P < 0.05$) (*SI Appendix*, Fig. S2*C*). Upon

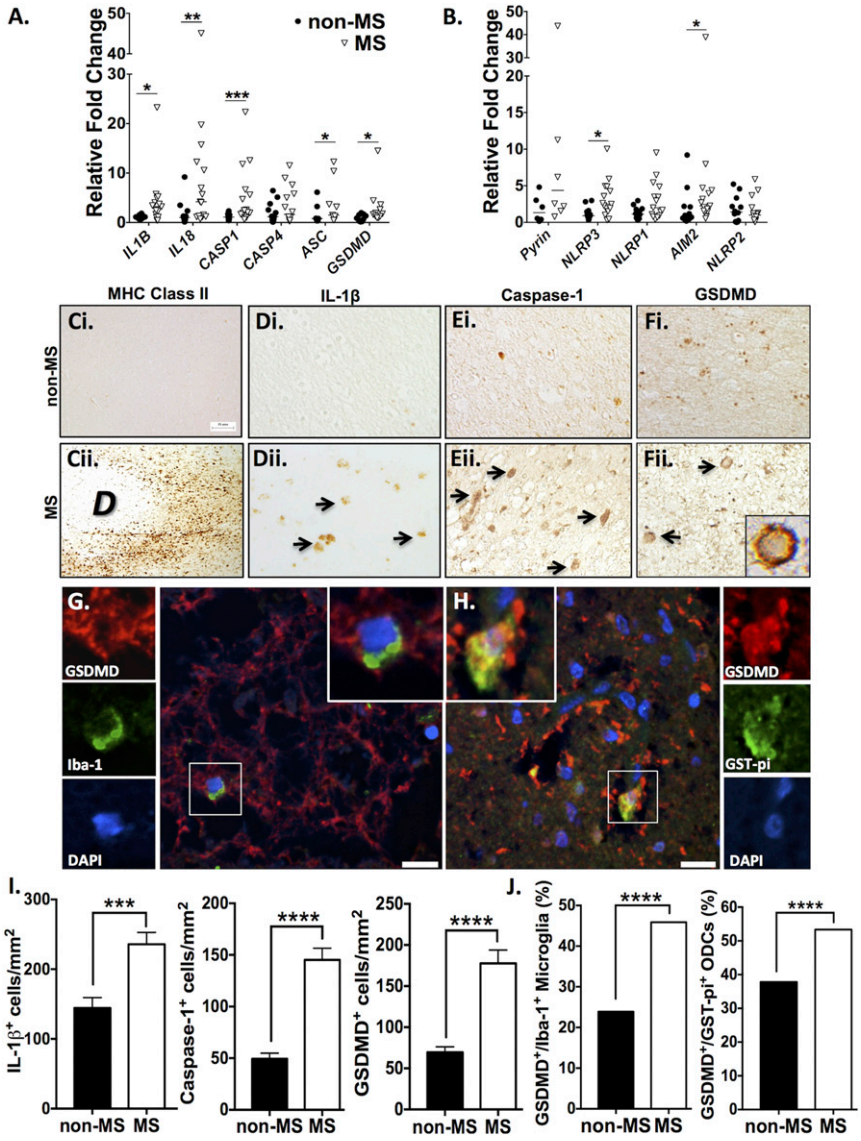

Fig. 1. Inflammasome- and pyroptosis-associated genes and proteins are up-regulated in the CNS of MS patients. (*A* and *B*) Transcript levels of inflammasome-associated genes were assessed using RT-PCR in MS ($n = 14$) and non-MS ($n = 10$) white matter autopsy samples. Values represent relative fold change compared with non-MS controls, with threshold cycles normalized to GAPDH (Mann–Whitney *U* test). (*C*–*F*) White matter was immunostained for proteins of interest, including MHC class II (*C*), IL-1β (*D*), caspase-1 (*E*), and GSDMD (*F*). (Magnification, 40×.) GSDMD immunoreactivity was localized to the plasma membrane of cells within MS lesions (*F*, *ii*, *Inset*). Arrows indicate positive cells. "*D*" indicates the area of demyelination. (*G*) Immunofluorescent labeling of macrophages/microglia in MS white matter with GSDMD (red), Iba-1 (green), and DAPI (blue) demonstrated GSDMD expression in Iba-1$^+$ cells. (*H*) Immunofluorescent labeling of ODCs in MS white matter with GSDMD (red), GST-pi (green), and DAPI (blue) demonstrated GSDMD expression in GST-pi$^+$ cells. (Scale bars in *G* and *H*, 13 μm.) (*I*) The number of IL-1β$^+$, caspase-1$^+$, and GSDMD$^+$ cells in white matter was quantified using a minimum of three MS and three non-MS autopsy samples, with a minimum of six nonoverlapping fields of view per patient. Data represent mean cell number per square millimeter ± SEM (Student's *t* test). (*J*) The proportion of GSDMD$^+$ microglia and ODCs was quantified. Proportions of microglia were calculated based on a minimum of 150 Iba-1$^+$ cells per group, using sections from two or three autopsy samples. Proportions of ODCs were calculated based on a minimum of 400 GST-pi$^+$ cells per group, using sections from two or three autopsy samples (χ^2 test). *$P < 0.05$, **$P < 0.01$, ***$P < 0.001$, ****$P < 0.0001$.

nigericin exposure, cell size also decreased ($P < 0.0001$) (Fig. 2*C*), which was accompanied by an increase in both IL-1β and GSDMD immunoreactivity ($P < 0.0001$) (Fig. 2 *D* and *E*).

To assess the effect of the caspase-1 inhibitor VX-765 on microglial pyroptosis, the proportion of microglia that demonstrated the characteristic ring-of-fire phenotype was quantified. While 19.6% of nigericin-exposed microglia displayed the phenotype, this diminished to 9.6% when microglia were pretreated with VX-765 ($P < 0.05$) (Fig. 2*F*). IL-1β (Fig. 2*G*) and IL-18 (Fig. 2*H*) release was also quantified following 24-h exposure to nigericin. Release of both cytokines was significantly reduced by VX-765 pretreatment in a concentration-dependent manner. IL-1β release was also inhibited by VX-765 ($P < 0.05$) at earlier time points (1 h and 4 h) (*SI Appendix*, Fig. S4*A*). In addition, nigericin exposure caused an increase in GSDMD and Il-1β immunoreactivity by immunoblot, which was diminished with VX-765 pretreatment (*SI Appendix*, Fig. S5). Full-length caspase-1 immunoreactivity was diminished with nigericin exposure, likely as a consequence of caspase-1 cleavage to form the p10 subunit upon activation; this effect was likewise inhibited by VX-765 (*SI Appendix*, Fig. S5 *A* and *C*). To quantify the loss of membrane integrity during pyroptosis, lactate dehydrogenase (LDH) activity was measured in cell culture supernatants, indicating extravasation of cellular contents. Nigericin exposure increased LDH release

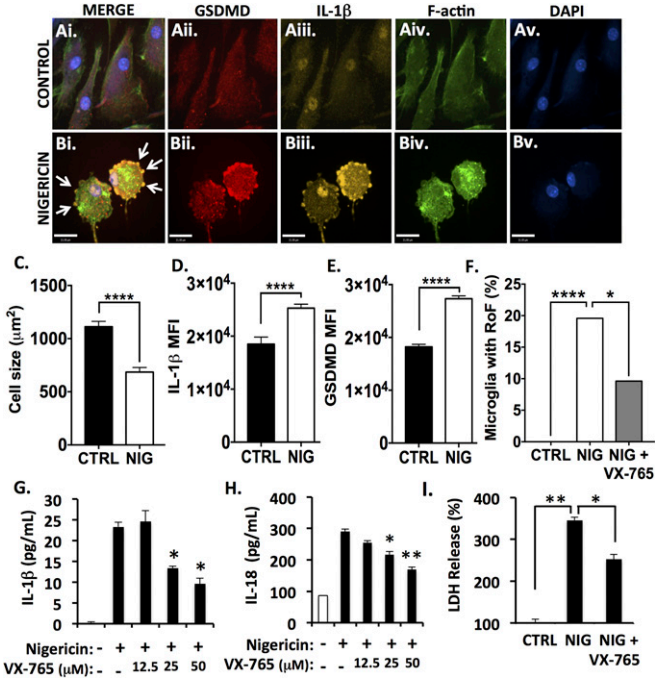

Fig. 2. Caspase-1 inhibition by VX-765 prevents inflammasome activation and pyroptosis in nigericin-exposed human microglia. Human microglia were exposed to nigericin (5 μM, 4 h) alone or following 4 h pretreatment with VX-765 (50 μM). (*A* and *B*) Control (*A*) and nigericin-exposed (*B*) microglia were immunolabeled for GSDMD (*A*, *ii* and *B*, *ii*) and IL-1β (*A*, *iii* and *B*, *iii*) and were labeled for F-actin (*A*, *iv* and *B*, *iv*). Nigericin-exposed microglia displayed the ring-of-fire phenotype characterized by a rounded morphology and the accumulation of GSDMD$^+$/IL-1β$^+$ pyroptotic bodies on the plasma membrane (arrows, *B*, *i*). (Scale bars, 23 μm.) (*C*) Cell size was quantified for 100–150 microglia per condition (control, CTRL, or nigericin-exposed, NIG). Data represent mean ± SEM and incorporate measurements from two biological donors. (*D* and *E*) IL-1β (*D*) and GSDMD (*E*) mean fluorescence intensity (MFI) was assessed. Data represent mean ± SEM and incorporate measurements from two biological donors. (*F*) To quantify the formation of the ring-of-fire phenotype, 100–150 microglia per condition were classified morphologically. Data represent the percentage of microglia demonstrating the phenotype and incorporate measurements from two biological donors (χ^2 test). (*G* and *H*) ELISA was used to assess IL-1β (*G*) and IL-18 (*H*) levels in supernatant from nigericin-exposed microglia. Data represent mean cytokine levels ± SEM (Student's *t* test). (*I*) Loss of cell membrane integrity was assessed using an LDH activity assay (Student's *t* test). LDH and ELISAs were performed with technical replicates of three to six wells per condition, and data were replicated in a minimum of three donor samples. *$P < 0.05$, **$P < 0.01$, ****$P < 0.0001$.

from microglia, while VX-765 treatment reduced its release in nigericin-exposed cells (Fig. 2*I*).

To verify GSDMD involvement in pyroptotic cell death, microglia were transfected with three GSDMD-targeting siRNAs or a universal negative siRNA. An average knockdown of 70% was achieved over multiple biological replicates, as measured by Western blot (*SI Appendix*, Fig. S6 *A* and *B*). This knockdown caused a significant ($P < 0.0001$) decrease in LDH release in nigericin-exposed GSDMD-knockdown microglia compared with microglia transfected with nontargeting siRNA (*SI Appendix*, Fig. S6*C*), thus verifying the role of GSDMD in microglial pyroptosis.

To investigate these phenomena with a more MS-relevant stimulus, comparable analyses were performed in microglia exposed to extracellular ATP (1 μM, 24 h). ATP is known to contribute to the neuropathology of EAE through ligation of the P2X7 receptor (34). ATP-exposed microglia also demonstrated a ring-of-fire phenotype including pyroptotic bodies (Fig. 3 *A* and *B*, white arrows). As with nigericin, exposure to ATP caused cellular rounding and shrinkage ($P < 0.0001$) (Fig. 3*C*) as well as an increase in both IL-1β and GSDMD intracellular immunoreactivity ($P < 0.0001$) (Fig. 3 *D* and *E*). At 24 h postexposure 11.9% of ATP-exposed microglia demonstrated the ring-of-fire phenotype, which dropped to 2.3% in the presence of VX-765 ($P < 0.05$) (Fig. 3*F*). As with nigericin, ATP-induced IL-1β release and LDH release were significantly reduced by VX-765 pretreatment ($P < 0.0001$). These observations indicated that VX-765 was an effective inhibitor of inflammasome activation and pyroptosis in microglia in response to biologically relevant stimuli. To assess whether GSDMD was equally important in ATP-induced microglial pyroptosis, microglia were transfected with three GSDMD-targeting siRNAs or a universal negative siRNA and were exposed to ATP with or without VX-765. LDH release was significantly ($P < 0.0001$) reduced in GSDMD siRNA-transfected ATP-treated microglia (*SI Appendix*, Fig. S6*D*) and was further reduced to baseline levels when GSDMD siRNA-transfected microglia were pretreated with VX-765 before ATP exposure. These data suggested that the combination of pharmacological caspase-1 inhibition (VX-765) and genetic GSDMD inhibition (siRNA) ameliorated ATP-induced pyroptosis.

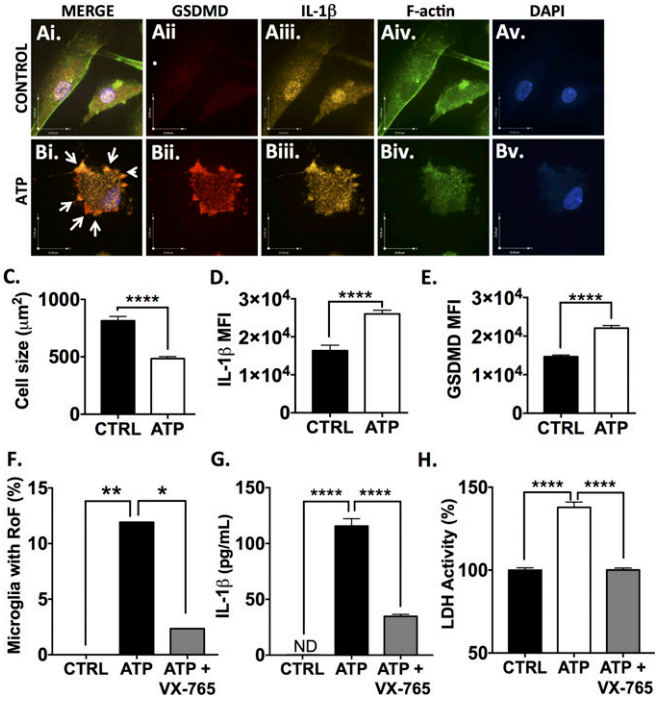

Fig. 3. VX-765 prevents inflammasome activation and pyroptosis in ATP-exposed human microglia. Human microglia were exposed to ATP (1 μM) alone or following pretreatment with VX-765 (50 μM, 4 h) for 24 h. (*A* and *B*) Control (*A*) and ATP-exposed (*B*) microglia were immunolabeled for GSDMD (*A*, *ii* and *B*, *ii*) and IL-1β (*A*, *iii* and *B*, *iii*) and were labeled for F-actin (*A*, *iv* and *B*, *iv*). ATP-treated microglia displayed the ring-of-fire phenotype characterized by a rounded morphology and the accumulation of GSDMD$^+$/IL-1β$^+$ pyroptotic bodies on the cell membrane (arrows, *B*, *i*). (Scale bars, 23 μm.) (*C*) Cell size was quantified for 80–150 microglia per condition. Data represent mean ± SEM. (*D* and *E*) IL-1β (*D*) and GSDMD (*E*) mean fluorescence intensity (MFI) was assessed for 80–150 microglia per condition. Data represent mean ± SEM. (*F*) To quantify the formation of the ring-of-fire phenotype, 80–150 microglia per condition were classified morphologically. Data represent the percentage of microglia demonstrating the phenotype (χ^2 test). RoF, ring of fire. (*G*) ELISA was used to assess IL-1β in supernatant from ATP-exposed microglia (1 μM ATP, 24 h). Data represent mean ± SEM (ANOVA). (*H*) Loss of cell membrane integrity was assessed by LDH activity assay (ANOVA). ELISA and LDH assays were performed with technical replicates of 6–12 wells per condition, and data were replicated in a minimum of three donor samples. *$P < 0.05$, ****$P < 0.0001$.

Inflammasome Activation and Pyroptosis in Human Oligodendrocytes. Given that GSDMD was also observed in ODCs near or within MS lesions, pyroptosis was assessed in undifferentiated progenitors and differentiated human ODCs in vitro. As ATP is nontoxic to ODCs (44), the cells were instead exposed to increasing concentrations of TNFα, an inflammasome-inducing cytokine with a well-established role in MS and known toxicity in ODCs (45).

TNFα concentration-dependent induction of pyroptosis-associated genes including *GSDMD* (Fig. 4*A*) and *CASP1* (Fig. 4*B*) was observed in differentiated (growth factor negative, GF^-) ODCs at 24 h postexposure ($P < 0.01$). Undifferentiated (growth factor positive, GF^+) progenitors, however, demonstrated minimal variations in *GSDMD* transcript levels and an increase in *CASP1* transcript levels in response to low-dose TNFα (*SI Appendix*, Fig. S7 *A* and *B*). These observations were recapitulated at the protein level: caspase-1 and GSDMD immunoreactivity in differentiated ODCs increased ($P < 0.0001$) in response to TNFα exposure (Fig. 4 *D* and *E*), but immunoreactivity was unchanged in TNFα-exposed progenitors (*SI Appendix*, Fig. S7 *F* and *G*). Interestingly, TNFα-induced GSDMD immunoreactivity was decreased with VX-765 pretreatment (Fig. 4*E*), suggesting a feedback loop in this model system whereby caspase-1 inhibition prevents further GSDMD up-regulation. Differentiated ODCs also displayed morphological changes associated with TNFα exposure (Fig. 4 *F*–*H*), including decreases in the number (Fig. 4*F*) and length (Fig. 4*G*) of processes ($P < 0.001$). These observations were accompanied by a TNFα-induced increase in the number of dysmorphic ODCs (defined by a condensed nucleus and few/no processes) in the population ($P < 0.001$). These changes were reversed by VX-765 treatment ($P < 0.001$), providing definitive evidence that these morphological changes were caspase-1–dependent.

Further evidence of nonapoptotic cell death included the release of extracellular LDH in differentiated TNF-α–exposed ODCs (*SI Appendix*, Fig. S8*F*). Interestingly, this phenotype was not associated with an increase in *IL1B* transcript levels (*SI Appendix*, Fig. S8*E*). Analysis of extrinsic apoptosis-related genes, including *CASP8*, *FADD*, *TRADD*, and *TRAF2*, also revealed a lack of induction at the transcript level (*SI Appendix*, Fig. S8 *A*–*D*), suggesting that ODC cell death was unlikely to be due to apoptosis.

CNS Inflammasome Activation in EAE. Although there is compelling evidence for inflammasome activation in the pathogenesis of EAE (25, 26), the implicated genes and their temporal expression profiles within the CNS were uncertain. Furthermore, it was imperative to establish whether the up-regulation of inflammasome genes observed in MS brains was recapitulated in the EAE model before considering CNS-targeted therapies to attenuate inflammasome activation. To address this issue, EAE was induced in C57/Bl6 mice using complete Freund's adjuvant (CFA)/$MOG_{35–55}$ with pertussis toxin, as previously reported by our group (46, 47), and tissues were collected at days 8 (preonset), 10 (onset), 15 (moderate disease), and 20 (peak disease) postinduction (PI) (Fig. 5 and *SI Appendix*, Figs. S9 and S10). Profiling hindbrain transcript levels by RT-PCR revealed a significant increase in *nlrp3* gene expression by day 8 PI, before onset of neurobehavioral deficits (Fig. 5*C*), followed by *il1b* (Fig. 5*A*), *casp11* (*SI Appendix*, Fig. S9*A*), and *pyrin* (*SI Appendix*, Fig. S9*B*) at day 10. *Casp1* expression was significantly increased (Fig. 5*B*) at day 15 and *gsdmd* at day 20 (Fig. 5*D*). Of note, *ifng* (*SI Appendix*, Fig. S10*E*) and *tnfa* (*SI Appendix*, Fig. S10*A*) were also significantly up-regulated in the hindbrain by day 10. *Nlrp1*, *nlrc4*, and *aim2* were significantly up-regulated at different points in the disease course (*SI Appendix*, Figs. S9 *C* and *E* and S10*G*), while *il18* was modestly up-regulated on day 15 (*SI Appendix*, Fig. S9*F*). Of note not all NOD-like receptors were induced: *nlrp6*, *nlrp2*, and *nlrp12* were unchanged (*SI Appendix*, Fig. S10 *B*, *D*, and *H*).

Oligodendrocytes and Myeloid Cells Undergo Pyroptosis in EAE. To extend the observations of GSDMD immunoreactivity and pyroptosis in human brains and cultured glial cells, spinal cords from CFA and EAE animals were examined, revealing an up-

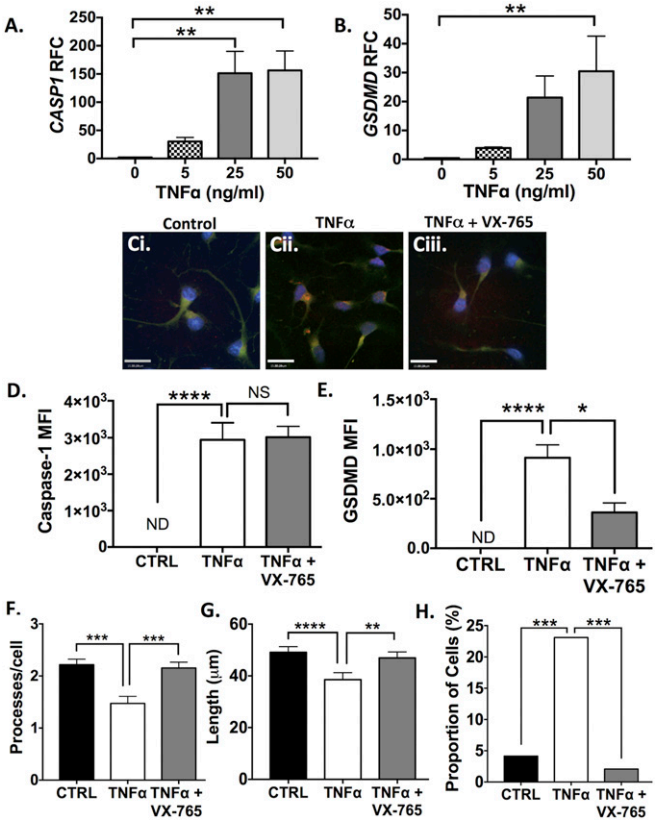

Fig. 4. TNFα exposure induces inflammasome activation and pyroptosis in human oligodendrocytes, which is rescued by VX-765. (*A* and *B*) Transcript levels of *CASP1* (*A*) and *GSDMD* (*B*) were assessed in differentiated ODCs after TNFα exposure (24 h, 50 ng/mL). Values represent relative fold change (RFC) compared with untreated controls, with threshold cycles normalized to GAPDH [three technical replicates per condition; mean ± SEM (ANOVA with Dunnett's multiple comparisons test)]. (*C*) Differentiated ODCs were exposed to TNFα for 24 h (50 ng/mL) with or without pretreatment with VX-765 (50 μM, 4 h) and were assessed by immunofluorescence. Upon TNFα exposure (*C*, *ii*), ODCs demonstrated loss or shortening of processes with enhanced GSDMD (red) and caspase-1 (green) immunoreactivity. (Scale bars, 15 μm.) (*D* and *E*) Mean fluorescence intensity (MFI) of caspase-1 (*D*) and GSDMD (*E*) was quantified (minimum 100 cells per condition). Average background fluorescence was subtracted from each value. Data represent mean MFI ± SEM (Kruskal–Wallis test with multiple comparisons). (*F* and *G*) To quantify morphological changes, the number (*F*) and length (*G*) of processes was quantified (minimum 200 cells per condition). Data represent the mean number and length of processes ± SEM (Kruskal–Wallis test with multiple comparisons). (*H*) The proportion of dysmorphic ODCs was quantified based on (*i*) condensed nucleus, (*ii*) few or no processes, (*iii*) positive for both f-actin and DAPI (minimum 180 cells per condition). Data represent the total proportion (%) of ODCs classified as dysmorphic within each treatment condition (χ^2 test). *$P < 0.05$, **$P < 0.01$, ***$P < 0.001$, ****$P < 0.0001$.

regulation of GSDMD (Fig. 5 *E*, *ii*, shown in green) in spinal cord lesions compared with CFA-exposed control animals (Fig. 5 *E*, *i*). GSDMD immunoreactivity was evident in Iba-1 immunopositive myeloid cells (Fig. 5 *E*, *iii*; Iba-1, red; overlap with green appears yellow/orange) as well as in cells that were not Iba-1 immunopositive (Fig. 5 *E*, *iv*). Lumbar spinal cord sections were then colabeled with antibodies to GSDMD and GST-pi, revealing GST-pi immunopositive ODCs (purple) with the characteristic GSDMD immunopositive ring at the cell surface (green) in lesions (Fig. 5 *F*, *i*–*v*). These double-immunopositive cells were usually proximal to Iba-1–immunopositive myeloid cells within the lesion (Fig. 5 *F*, *i*, red), some of which were also GSDMD-immunopositive (green; overlap appears yellow).

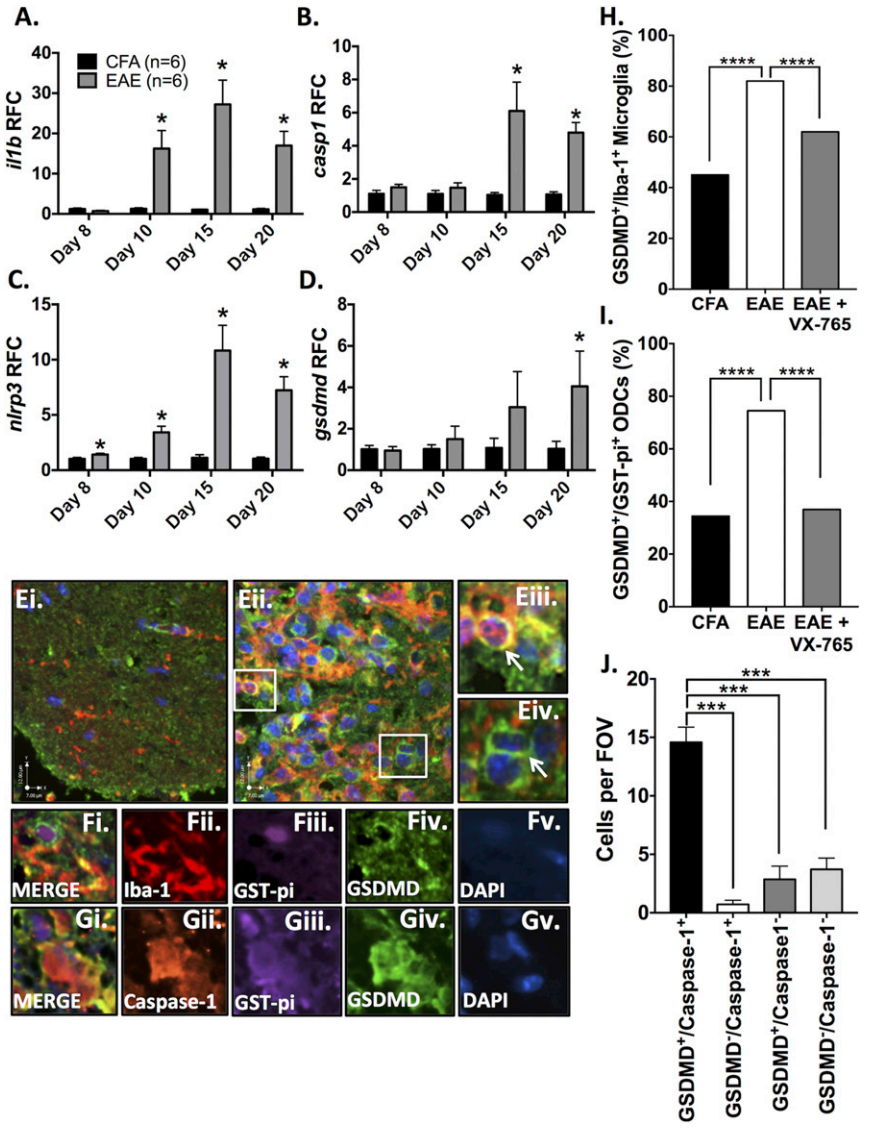

Fig. 5. Inflammasome activation and pyroptosis in the CNS during EAE. Control (CFA) and EAE (MOG) C57Bl6 mice were killed on day 8 (preonset), day 10 (onset), day 15 (mid-disease), and day 20 (peak disease) ($n = 6$ mice per group per time point). (*A–D*) Hindbrain transcript levels of *il1b* (*A*), *casp1* (*B*), *nlrp3* (*C*), and *gsdmd* (*D*) were assessed using real-time RT-PCR. Data represent relative fold change (RFC) compared with CFA controls, normalized to *hprt*. (*E*) Immunofluorescent labeling of lumbar spinal cord at peak disease was performed. GSDMD is shown in green, and Iba-1 is shown in red. While CFA-exposed control animals demonstrated minimal GSDMD (*E*, *i*; green) and only trace numbers of Iba-1$^+$ cells (*E*, *i*, red), EAE animals (*E*, *ii*) demonstrated intense GSDMD immunostaining and a profound increase in Iba-1$^+$ cells in spinal cord lesions. GSDMD immunoreactivity was observed in Iba-1$^+$ cells (*E*, *iii*; overlap appears yellow), but other GSDMD$^+$ cells were Iba-1$^-$ (*E*, *iv*). (*F*) Immunofluorescent triple labeling of EAE spinal cords from peak disease with GST-pi (*F*, *iii*; purple) revealed rings of GSDMD immunostaining (*F*, *iv*; green) on ODCs within spinal cord lesions. GSDMD$^+$ ODCs (*F*, *i*) were often found near activated microglia. (*G*) Immunofluorescent triple labeling of EAE spinal cords [GST-pi (*G*, *iii*, purple), GSDMD (*G*, *iv*, green), and caspase-1 (*G*, *ii*, red)] showed both pyroptosis markers within GST-pi$^+$ cells. (Scale bars, 7 μm horizontal and 12 μm vertical.) (*H*) The proportion of GSDMD$^+$ microglia and ODCs in the ventral lumbar spinal cord was quantified. Data represent the proportion of GSDMD$^+$/Iba-1$^+$ cells (%) as a fraction of Iba-1$^+$ cells. Proportions were calculated using up to 500 Iba-1$^+$ cells per condition, with multiple spinal cord sections from two or three representative animals per condition (χ^2 test). (*I*) Data represent the proportion of GSDMD$^+$/GST-pi$^+$ ODCs (%) as a fraction of GST-pi$^+$ ODCs. Proportions were calculated based on analysis of up to 400 GST-pi$^+$ cells per condition using multiple spinal cord sections from two or three animals per condition (χ^2 test). (*J*) To determine if caspase-1 was found within GSDMD$^+$ ODCs, over 150 GST-pi$^+$ ventral column ODCs from EAE animals at peak disease were classified as double-positive (GSDMD$^+$/caspase-1$^+$), single-positive (GSDMD$^+$/caspase-1$^-$ or GSDMD$^-$/caspase-1$^+$), or double-negative (GSDMD$^-$/caspase-1$^-$). Data represent mean number of cells per field of view ± SEM (ANOVA). ***$P < 0.001$, ****$P < 0.0001$. FOV, field of view.

In high-magnification images (*SI Appendix*, Fig. S11), microglia undergoing pyroptosis displayed GSDMD expression around the cell periphery, large dysmorphic nuclei, and only moderate Iba-1 expression. The inflammatory nature of this cell-death process was highlighted by the recruitment of GSDMD$^-$ Iba-1$^+$ reactive microglia (yellow arrows) in close proximity to GSDMD$^+$ microglia undergoing pyroptosis (white arrows).

To quantify these findings, the proportions of GSDMD$^+$ microglia and ODCs in the ventral spinal column were assessed. Similar to MS patients, EAE animals displayed a significant ($P < 0.0001$) increase in the proportion of both microglia and ODCs immunopositive for GSDMD.

We next determined whether GSDMD was expressed in ODCs coexpressing caspase-1, diminishing the likelihood that GSDMD was playing a non–inflammasome-related role in ODCs in vivo. To this end, immunofluorescent triple labeling was performed to assess caspase-1, GSDMD, and GST-pi immunoreactivity simultaneously (Fig. 5 *G*, *i–v*), revealing multiple GST-pi immunopositive

cells (Fig. 5 *G*, *iii*, purple) that were also positive for both GSDMD (Fig. 5 *G*, *iv*, green) and caspase-1 (Fig. 5 *G*, *ii*, red). The majority of GST-pi$^+$ ODCs in the ventral spinal cords from EAE animals were double immunopositive for GSDMD and caspase-1 ($P < 0.001$) (Fig. 5*J*). GSDMD-immunopositive astrocytes or neurons were not observed in the lumbar spinal cord during EAE (*SI Appendix*, Fig. S12).

EAE-Associated Neuropathology Is Diminished by VX-765 Treatment. Given the striking changes in CNS inflammasome protein expression in EAE and the evidence for pyroptosis in both myeloid and nonmyeloid cells in the CNS, inhibition of caspase-1 with VX-765 was a logical experimental approach. To determine whether VX-765 treatment influenced disease outcomes, EAE animals were treated with VX-765 (50 mg/kg i.p.) daily or with vehicle (PBS/DMSO). To recapitulate clinical circumstances, VX-765 or vehicle treatment was initiated after neurobehavioral deficits were observed (day 12 PI).

Morphological analyses of spinal cords from each group were performed by immunohistochemistry and immunofluorescence, concentrating on the ventral columns because they largely mediate motor functions. Compared with PBS/DMSO-treated animals, the proportion of GSDMD$^+$ microglia and oligodendrocytes decreased ($P < 0.0001$) upon treatment with VX-765 (Fig. 5 *H* and *I*).

Further immunohistochemistry studies revealed that parenchymal Iba-1 immunoreactivity was detected in ventral spinal cord white matter of CFA-exposed animals (Fig. 6 *A*, *i*) but was markedly increased in EAE animals (Fig. 6 *A*, *ii*). VX-765 treatment attenuated myeloid cell activation as indicated by Iba-1 immunoreactivity (Fig. 6 *A*, *iii*) (quantification is shown in *SI Appendix*, Fig. S13). IL-1β immunoreactivity was minimal in CFA-exposed animals (Fig. 6 *B*, *i*) and was induced in EAE spinal cords (Fig. 6 *B*, *ii*), compared with VX-765-treated animals ($P < 0.0001$) (Fig. 6 *B*, *iii*; quantified in Fig. 6*E*). Caspase-1 immunoreactivity was also limited in CFA-exposed animals (Fig. 6 *C*, *i*) and increased in vehicle-treated EAE animals (Fig. 6 *C*, *ii*), but again caspase-1 expression was reduced with VX-765 treatment ($P < 0.0001$, quantified in Fig. 6*F*). GSDMD expression was minimal in the spinal cords of CFA-exposed animals (Fig. 6 *D*, *i*) but was enhanced in the spinal cords of EAE animals. Notably, cells displayed GSDMD immunoreactivity at the plasma membrane (Fig. 6 *D*, *ii*, *Inset*), consistent with pyroptosis. VX-765 treatment suppressed GSDMD immunoreactivity ($P < 0.0001$) (Fig. 6 *D*, *iii*; quantified in Fig. 6*G*).

VX-765 Treatment Reduces CNS Inflammation, Prevents Axonal Injury, and Improves Neurobehavioral Outcomes in EAE. Evaluation of transcript levels in spinal cord at day 20 PI revealed that *il1b* (Fig. 7*A*), *nlrp3* (Fig. 7*B*), and *casp1* (Fig. 7*C*) were highly induced in the spinal cords of vehicle-treated EAE animals, but VX-765 treatment abrogated the induction of *nlrp3* and *casp1*. Additionally, other genes, including *pyrin*, *ifng*, and *tnfa*, were also suppressed in VX-765-treated EAE animals (Fig. 7*D*). These data indicated that VX-765 treatment reduced the expression of several key inflammasome- and inflammation-related genes in the CNS, pointing to an overall suppression of neuroinflammation.

Axonal integrity was assessed by Bielchowsky's silver staining in the ventral columns of spinal cords from the CFA, EAE + PBS, and EAE + VX-765 treatment groups. Densely stained silver-positive axons were observed in the CFA-exposed animals (Fig. 7*E*), while fewer silver-positive axons were detected in the EAE group (Fig. 7*F*); VX-765 treatment preserved axonal density (Fig. 7 *G* and *H*). The density of motor neurons in the ventral horn was also quantified, indicating a loss of motor neurons in EAE animals at peak disease ($P < 0.05$) which was prevented by VX-765 treatment ($P < 0.05$) (*SI Appendix*, Fig. S14).

In addition to the molecular and neuropathological findings indicating that inflammasome activation in EAE was suppressed by VX-765 treatment, neurobehavioral assessment permitted serial analyses of the effects of the therapeutic intervention. VX-765 treatment reduced the severity of neurobehavioral deficits by day 15 PI (after only 3 d of treatment) compared with vehicle-treated EAE animals, which was sustained for most of the experiment (Fig. 7*I*). Thus, VX-765 treatment exerted significant and sustained beneficial effects on EAE-associated neurobehavioral deficits in conjunction with reduced CNS inflammasome activity.

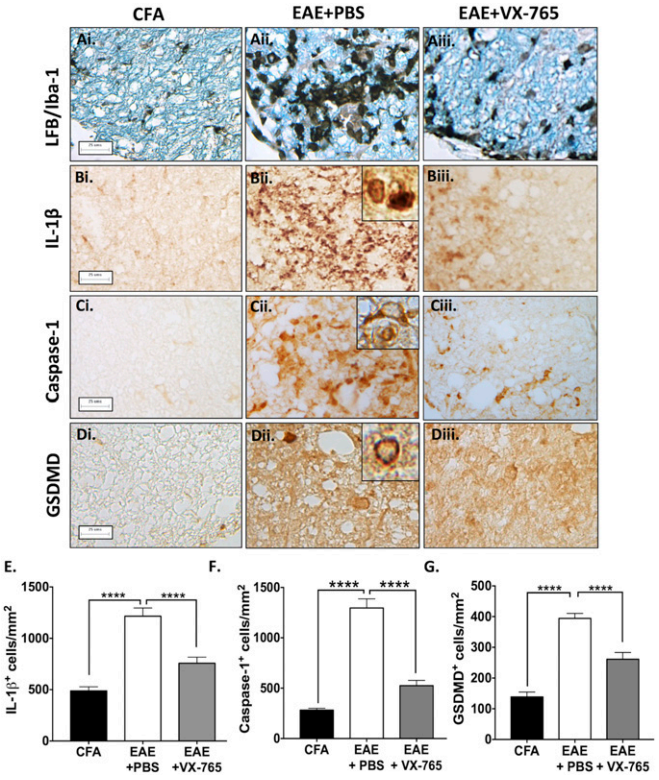

Fig. 6. Reduced inflammasome- and pyroptosis-associated protein expression with VX-765 treatment in EAE. (*A*) Lumbar spinal cords from control (CFA) and EAE mice treated with either vehicle (EAE+PBS) or VX-765 (EAE+VX-765) and killed at peak disease were labeled with Luxol Fast Blue stain for myelin (LFB) and Iba-1. Accumulation of myeloid cells was evident in ventral column lesions of the EAE+PBS-treated group (*A*, *ii*), which was markedly diminished in VX-765–treated animals (*A*, *iii*). (Scale bars: 25 μm.) (Magnification of *Insets*: 60×.) (*B*) Localized accumulation of IL-1β$^+$ cells was observed in PBS-treated EAE animals (*B*, *ii*, *Inset*), which decreased in VX-765–treated mice (*B*, *iii*). (*C*) Enhanced caspase-1 immunoreactivity was evident in cytoplasm of cells in ventral column lesions in EAE+PBS mice (*C*, *ii*, *Inset*) but was diminished with VX-765 treatment (*C*, *iii*). (*D*) GSDMD immunoreactivity was observed in the spinal cords of EAE+PBS mice (*D*, *ii*) and to a lesser extent in VX-765-treated mice (*D*, *iii*). Localization of GSDMD to the plasma membrane, indicative of pyroptosis, was observed in PBS-treated animals (*D*, *ii*, *Inset*). (*E*–*G*) The number of IL-1β$^+$ (*E*), caspase-1$^+$ (*F*), and GSDMD$^+$ (*G*) cells in the ventral spinal cord from CFA, EAE + PBS, and EAE + VX-765 animals was quantified. Immunohistochemical quantification was performed using multiple spinal cord sections from two or three animals per experimental group with a minimum of 10 nonoverlapping fields of view per animal. Data represent the mean cell number per square millimeter ± SEM (ANOVA). ****$P < 0.0001$.

Discussion

This report provides compelling evidence for inflammasome activation and pyroptosis in both ODCs and microglia during inflammatory demyelination. Morphological and molecular evidence of pyroptosis was observed in the CNS in both MS and EAE, indicated by caspase-1 immunoreactivity and GSDMD accumulation on the plasma membrane forming a distinctive ring of fire (Figs. 1 and 6). This appearance mirrored that of human microglia undergoing pyroptosis in vitro, evidenced by the aggregation of GSDMD at the plasma membrane, release of inflammasome-associated cytokines, and extravasation of cellular contents (Figs. 2 and 3), all of which were prevented by

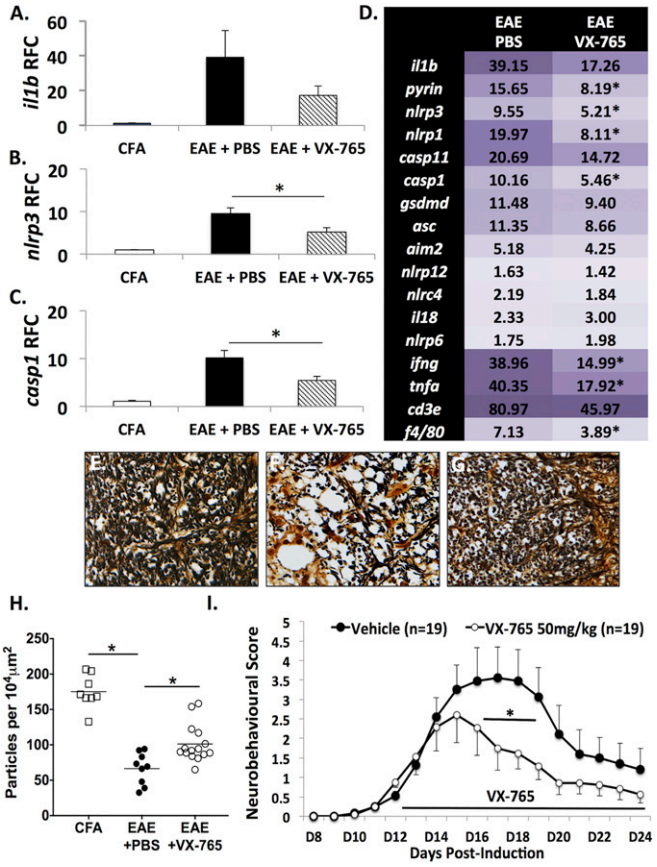

Fig. 7. VX-765 treatment reduces neuroinflammation, protects spinal cord axons, and improves neurobehavioral outcomes in EAE. (*A–C*) *il1b* (*A*), *nlrp3* (*B*), and *casp1* (*C*) gene expression was assessed by RT-PCR at peak disease in lumbar spinal cords of EAE animals treated with VX-765 ($n = 9$) or vehicle control ($n = 9$). (*D*) Other inflammatory genes implicated in EAE pathogenesis showed altered expression in EAE spinal cords with VX-765 treatment. Values represent mean relative fold change compared with CFA controls, with threshold cycle normalized to the housekeeping gene *hprt* ($n = 6$). (Student's *t* test). (*E–G*) Silver staining of lumbar spinal cord axons from CFA-exposed controls (*E*), EAE+PBS mice (*F*), and EAE+VX-765 mice (*G*) revealed loss of axons in the ventral column of the spinal cord compared with CFA-treated controls. (Magnification: 40×.) (*H*) VX-765 treatment resulted in the preservation of axons ($n = 2–3$ animals per group, four to five fields of view per animal). Quantification of axonal density was expressed as particles per 10,000 μm^2 and showed axonal density was significantly reduced in PBS-treated EAE animals. This effect was partially rescued with VX-765 treatment. (*I*) Neurobehavioral signs were scored daily, and VX-765 treatment was initiated after the onset of tail paralysis (day 12). VX-765 treatment ($n = 19$) reduced EAE-associated neurobehavioral deficits compared with vehicle-treated EAE animals ($n = 19$) (ANOVA with Bonferroni correction). $^*P < 0.05$.

pretreatment with the caspase-1 inhibitor VX-765. ODCs also demonstrated evidence of pyroptosis, albeit in the absence of inflammasome-associated cytokine release, thus representing an alternative paradigm in which IL-1β synthesis is not coincident with pyroptotic cell death. Treatment of EAE animals with VX-765 improved neurobehavioral performance, reduced neuropathological severity, and diminished molecular indicators of inflammation (Figs. 6 and 7). Taken together, the present observations defined a distinctive CNS inflammasome profile for MS and EAE, yielded the discovery of pyroptosis in microglia and ODCs during demyelination, and illustrated the potential therapeutic impact of caspase-1 inhibition using VX-765.

We propose a model in which dying ODCs release DAMPs that activate inflammasomes in resident microglia and infiltrating macrophages (*SI Appendix*, Fig. S15). These activated myeloid cells release both non–inflammasome-dependent cytokines (e.g., TNFα) and inflammasome-dependent cytokines (IL-1β and IL-18), which drive a persistent inflammatory cascade that activates infiltrating lymphocytes and causes neuronal and axonal toxicity. A subset of microglia/macrophages also undergoes pyroptosis, which further amplifies pathology through the release of neurotoxic and inflammatory mediators (e.g., cytokines, reactive oxygen species) and intracellular DAMPs, many of which have recognized off-target effects on neurons and oligodendrocytes. TNFα released from activated microglia/macrophages promotes GSDMD upregulation and pyroptosis in ODCs, further exacerbating tissue loss and demyelination. By inhibiting caspase-1, VX-765 blocks inflammasome signaling, reduces cytokine-associated neurotoxicity, and prevents GSDMD-mediated pyroptosis in both myeloid cells and ODCs, leading to tissue preservation and improved disease outcome.

While macrophage/microglia cell death has not been extensively characterized in MS, signs of cell degeneration in iron-containing microglia have been observed (48); this phenomenon has likely been underappreciated due to an influx of infiltrating blood-derived macrophages. Our observation of myeloid cells with the prototypic ring of GSDMD immunoreactivity within MS and EAE lesions (Figs. 1, 5, and 6) suggested that myeloid cells might undergo pyroptosis in the diseased brain, amplifying MS pathogenesis through the concomitant release of neurotoxic and inflammatory mediators and intracellular DAMPs. Targeting microglial pyroptosis therapeutically might thus exert neuroprotective effects by preventing extravasation of cytotoxic molecules.

By contrast, damaged and dying ODCs in MS lesions are well characterized, and have been shown to express apoptotic markers (e.g., TUNEL and cleaved caspase-3), leading to the conclusion that apoptosis was at least partially responsible for ODC death (49). Recently, RIPK1-dependent necroptosis was also proposed as a mechanism for ODC degeneration, particularly in gray matter in MS (50). The present study implicating pyroptosis in ODCs highlights the possibility that multiple cell death pathways may drive demyelination. Furthermore, certain apoptosis markers are now understood to be nonspecific; for instance, it has been shown that TUNEL labels cells undergoing both necroptosis (51) and pyroptosis (52), and cleaved caspase-3 can activate pyroptosis rather than apoptosis through the related protein gasdermin E (53). This raises the possibility that ODC death previously attributed to apoptosis or necroptosis might alternatively represent pyroptosis. Targeting GSDMD or upstream proinflammatory caspases, as shown herein, represents a paradigm-changing strategy to promote neuroprotection. Attempts to therapeutically target inflammasome-associated cytokines in MS without targeting the pathways mediating cell death might have limited efficacy, as cytokine release appears to be dispensable for ODC pyroptosis. Furthermore, understanding caspase-mediated pyroptosis might enable the development of highly targeted approaches to mitigate neuroinflammation and promote neuroprotection in the clinical setting.

CNS inflammasome activation contributes to neuropathology through multiple mechanisms beyond pyroptosis. IL-1β and IL-18 exert neurotoxic effects and activate lymphocytes infiltrating into the CNS (18, 54, 55). IL-1β enhances glutamate excitotoxicity in MS (56). Given the well-defined role of IL-1β in the CNS during MS and EAE, inflammasome inhibition with VX-765 is a particularly apt choice, because it has been used with an acceptable safety profile in clinical trials for psoriasis (57) and epilepsy (58). Brain penetrance data are also available for rodent models, verifying that it crosses the blood–brain barrier (59).

Another mechanism by which VX-765 might diminish EAE disease severity is through inflammasome inhibition in the peripheral (non-CNS) compartment. IL-18 and IL-1β promote autoreactive T cell priming and Th17 cell development and prime the endothelium for extravasation of immune cells during EAE (39, 60–62). To minimize VX-765's effects on the peripheral response in our studies, daily VX-765 treatment was initiated after the onset of neurobehavioral signs, at which point CNS infiltration of pathogenic lymphocytes was underway.

Although *ifng* was significantly reduced and *cd3e* trended downward in the CNS of VX-765–treated animals compared with vehicle-treated mice at peak disease, VX-765 did not block T cell infiltration; *ifng* remained up-regulated (15-fold) in the CNS compared with CFA controls, while *cd3e* was still induced (46-fold) in VX-765–treated animals compared with CFA controls (Fig. 7*D*). These findings implied that the efficacy of VX-765 could not be explained solely by effects on T cell infiltration. Phytohemagglutinin/IL-2–activated human lymphocytes also failed to show cytotoxicity with VX-765 treatment (*SI Appendix*, Fig. S16), making T cell toxicity unlikely to be a protective mechanism during EAE. Furthermore, no inflammasome activation was detected in the spleens of EAE animals at peak disease (*SI Appendix*, Fig. S17). These observations suggest that VX-765's therapeutic efficacy was not attributable to its effects on lymphocyte viability or inflammasome activation outside the CNS. Nonetheless, a more direct administration route, such as intraventricular or intrathecal administration of VX-765, might clarify this issue. From a clinical perspective, we anticipate that any effects of VX-765 on peripheral rather than CNS inflammasome activation would further attenuate the disease, given the well-established role of inflammasome-associated cytokines in T cell priming, migration, and CNS infiltration.

Several issues remain unanswered by the present studies, including the relative contribution of peripheral versus CNS inflammasome activation to disease pathology. This dilemma is not addressed by contemporary inflammasome-null mouse models, in which both peripheral and CNS inflammasome functions are impacted. Recent studies using the cuprizone model of demyelination in several inflammasome-null mouse models overcome this issue, as cuprizone does not have a peripheral autoimmune component (15). The potential off-target effects of VX-765 are also an issue in terms of interpreting the current results, but the consistency of inflammasome inhibition points to a specific effect largely directed at CNS inflammasome activation. Finally, the contributions of GSDMD and related gasdermins to MS pathogenesis await deeper analyses using null mice and more targeted therapeutic compounds as these reagents become available.

In summary, inflammasome activation and pyroptosis represent therapeutically targetable and previously unrecognized mechanisms driving neuroinflammation and neurodegeneration in MS. Molecular profiles of CNS inflammasome activation were similar in MS and EAE. These findings were complemented by evidence pointing to pyroptosis, mediated by GSDMD translocation to the plasma membrane, in both microglia/macrophages and ODCs. Inhibition of proinflammatory caspase activation using VX-765 resulted in reduced inflammasome activation and yielded improved outcomes in EAE. Collectively, these findings offer unique perspectives on MS pathogenesis and its treatment options.

Materials and Methods

Ethics Statement. Use of autopsied tissues was approved (Pro0002291) by the University of Alberta Human Research Ethics Board (Biomedical), and written informed consent was received for all samples (*SI Appendix*, Table S1). Human fetal tissues were obtained from 15- to 22-wk aborted fetuses collected with written informed consent of the donor (Pro00027660), as approved by the University of Alberta Human Research Ethics Board (Biomedical). Animal experiments were performed according to Canadian Council on Animal Care and University of Alberta Health Sciences Animal Care and Use Committee guidelines.

Primary Cell Cultures. Primary fetal human microglia were isolated based on differential culture conditions, as previously described (43, 63). Progenitor-derived oligodendrocytes were derived as previously described (64). See *SI Appendix* for details.

Ex Vivo Inflammasome Activation and Modulation. Microglia were exposed to nigericin (5 μM; catalog no. tlrl-nig; InvivoGen), ATP-γ-S [1 μM, adenosine 5′-O-(3-thiotriphosphate), a thiophosphorylated phosphatase-resistant form of ATP; catalog no. 11162306001; Sigma-Aldrich], either ATP or nigericin plus VX-765 (50 μM, 4 h pretreatment, catalog no. inh-vx765-1; InvivoGen), or solvent control for 4 or 24 h as indicated. Supernatants were harvested and stored at −80 °C.

siRNA Knockdown of GSDMD. Cells were transfected with 30 nM of non-targeting siRNA (TriFECTa RNAi Kit; Integrated DNA Technologies) or a mixture of three commercially available GSDMD-targeting Dicer-Substrate siRNAs (30 nM), in combination with PrecisionFectin Transfection Reagent (BioIntersect). After 48 h, cells were exposed to nigericin, ATP, or solvent control (with or without VX-765) for 24 h.

Western Blot Analysis. Immunoblot analysis of cell lysates was performed as described previously (47, 65). See *SI Appendix* for details.

ELISAs. IL-1β assays were performed using the Human IL-1β DuoSet ELISA kit (DY201; R&D Systems). IL-18 assays were performed using the Thermo Fisher IL-18 Human Instant ELISA kit (BMS267INST) as described previously (43, 65).

LDH Assay. LDH activity in cell supernatants was assessed using LDH-Cytotoxicity Assay Kit II (ab65393; Abcam). Briefly, microglia were plated in 96-well plates before exposure to nigericin (5 μM), ATP (1 μM), nigericin or ATP plus VX-765 (4 h pretreatment; 50 μM), or solvent control (PBS) for 24 h. Supernatants were harvested and stored at −80 °C before use.

Cell Culture Immunofluorescence. Detection of cellular proteins was performed using immunofluorescence as described previously (65). Slides were imaged using a Wave FX spinning-disk confocal microscope (Zeiss) with Volocity 6.3 acquisition and analysis software (PerkinElmer). See *SI Appendix* for details.

PCR. Total RNA was extracted using TRIzol (Invitrogen); cDNA was generated and subjected to semiquantitative PCR using verified primers (*SI Appendix*, Tables S1 and S2) as previously described (43, 65). Details are available in *SI Appendix*.

EAE Induction and Monitoring. C57BL/6 female mice (10–12 wk old) were immunized with $MOG_{35–55}$ peptide (1 mg/mL) emulsified with CFA (EK-0115/EK-2110; Hooke Laboratories) and injected with pertussis toxin (200 ng per mouse) (47). Animals were fed a Bio-Serv Nutra-Gel diet (no. F4798-KIT; Bio-Serv) to reduce dehydration. Several different EAE experiments were performed. To analyze time-dependent up-regulation of inflammasome-related genes, CFA and MOG animals were killed at day 8, 10, 15, and 20, and hindbrains were collected for PCR. To analyze the effect of VX-765 on neurobehavioral and neuropathological outcomes, EAE animals received daily i.p. injections of VX-765 (50 mg/kg) diluted in PBS/DMSO from the onset of clinical signs (day 12) until the end of the experiment. Vehicle-treated animals received daily injections of PBS/DMSO. CFA animals were untreated. EAE animals were assessed daily and scored for disease severity up to 24 d following EAE induction using an established 0–15 point scale (66). Hindbrains and spinal cords were collected for PCR, immunohistochemistry, and histopathological and immunofluorescence analysis.

Immunofluorescence, Immunohistochemistry, and Histochemistry. Human brain tissue was fixed in 10% formalin. Paraffin-embedded sections (10 μm) were prepared for histological and immunolabeling studies. Mice were killed, and transcardiac perfusion was performed with PBS. Spinal cords were dissected, fixed in 4% paraformaldehyde, and processed for paraffin embedding and sectioning (10 μm). Axonal counting was performed based on Bielchowsky's silver staining and quantified using FIJI (67). Immunohistochemical and immunofluorescent labeling of human and mouse CNS tissues was performed as previously reported (47). Details and quantification procedures are available in *SI Appendix*.

Statistical Analyses. Statistical analyses for clinical samples were performed using the Mann–Whitney u test. A χ^2 test was used to compare proportions of double-positive cells for immunofluorescence studies. Comparisons between two groups were performed by unpaired Student's *t* test or by ANOVA with Tukey–Kramer or Bonferroni post hoc tests, using GraphPad Instat 3.0 (GraphPad Software).

ACKNOWLEDGMENTS. We thank Drs. John G. Walsh, Kris Ellestad, Nathalie Arbour, Daniel Muruve, and the Cell Imaging Centre at the University of Alberta for helpful discussions. B.A.M. is supported by the Canadian Institutes of Health Research, Alberta Innovates (AI), and a Queen Elizabeth II

Doctoral Scholarship. M.K.M. holds fellowship awards from Campus Alberta Neuroscience and AI. L.B.S. is supported by the Multiple Sclerosis Society of Canada (MSSoC). C.P. holds a Canada Research Chair in Neurological Infection and Immunity. These studies were supported by the MSSoC, University Hospital Foundation, and Canada Foundation for Innovation (C.P.).

1. Martinon F, Burns K, Tschopp J (2002) The inflammasome: A molecular platform triggering activation of inflammatory caspases and processing of proIL-beta. *Mol Cell* 10:417–426.
2. Latz E, Xiao TS, Stutz A (2013) Activation and regulation of the inflammasomes. *Nat Rev Immunol* 13:397–411.
3. Álvarez S, Muñoz-Fernández MA (2013) TNF-A may mediate inflammasome activation in the absence of bacterial infection in more than one way. *PLoS One* 8:e71477.
4. Broz P, Dixit VM (2016) Inflammasomes: Mechanism of assembly, regulation and signalling. *Nat Rev Immunol* 16:407–420.
5. Lawrence T (2009) The nuclear factor NF-kappaB pathway in inflammation. *Cold Spring Harb Perspect Biol* 1:a001651.
6. O'Neill LA, Greene C (1998) Signal transduction pathways activated by the IL-1 receptor family: Ancient signaling machinery in mammals, insects, and plants. *J Leukoc Biol* 63:650–657.
7. Aglietti RA, Dueber EC (2017) Recent insights into the molecular mechanisms underlying pyroptosis and gasdermin family functions. *Trends Immunol* 38:261–271.
8. Ding J, et al. (2016) Pore-forming activity and structural autoinhibition of the gasdermin family. *Nature* 535:111–116.
9. Shi J, et al. (2015) Cleavage of GSDMD by inflammatory caspases determines pyroptotic cell death. *Nature* 526:660–665.
10. Liu X, et al. (2016) Inflammasome-activated gasdermin D causes pyroptosis by forming membrane pores. *Nature* 535:153–158.
11. Kayagaki N, et al. (2015) Caspase-11 cleaves gasdermin D for non-canonical inflammasome signalling. *Nature* 526:666–671.
12. Walsh JG, Muruve DA, Power C (2014) Inflammasomes in the CNS. *Nat Rev Neurosci* 15:84–97.
13. Kaushal V, et al. (2015) Neuronal NLRP1 inflammasome activation of caspase-1 coordinately regulates inflammatory interleukin-1-beta production and axonal degeneration-associated caspase-6 activation. *Cell Death Differ* 22:1676–1686.
14. Minkiewicz J, de Rivero Vaccari JP, Keane RW (2013) Human astrocytes express a novel NLRP2 inflammasome. *Glia* 61:1113–1121.
15. Freeman L, et al. (2017) NLR members NLRC4 and NLRP3 mediate sterile inflammasome activation in microglia and astrocytes. *J Exp Med* 214:1351–1370.
16. Alboni S, Cervia D, Sugama S, Conti B (2010) Interleukin 18 in the CNS. *J Neuroinflammation* 7:9.
17. Hein AM, et al. (2010) Sustained hippocampal IL-1beta overexpression impairs contextual and spatial memory in transgenic mice. *Brain Behav Immun* 24:243–253.
18. Lee PR, et al. (2017) Protease-activated receptor-1 activation by granzyme B causes neurotoxicity that is augmented by interleukin-1β. *J Neuroinflammation* 14:131.
19. Freeman LC, Ting JP (2016) The pathogenic role of the inflammasome in neurodegenerative diseases. *J Neurochem* 136:29–38.
20. Mamik MK, Power C (2017) Inflammasomes in neurological diseases: Emerging pathogenic and therapeutic concepts. *Brain* 140:2273–2285.
21. Dendrou CA, Fugger L, Friese MA (2015) Immunopathology of multiple sclerosis. *Nat Rev Immunol* 15:545–558.
22. Kornek B, Lassmann H (2003) Neuropathology of multiple sclerosis-new concepts. *Brain Res Bull* 61:321–326.
23. Hemmer B, Kerschensteiner M, Korn T (2015) Role of the innate and adaptive immune responses in the course of multiple sclerosis. *Lancet Neurol* 14:406–419.
24. Kuhlmann T, et al. (2017) An updated histological classification system for multiple sclerosis lesions. *Acta Neuropathol* 133:13–24.
25. Barclay W, Shinohara ML (2017) Inflammasome activation in multiple sclerosis and experimental autoimmune encephalomyelitis (EAE). *Brain Pathol* 27:213–219.
26. Inoue M, Shinohara ML (2013) NLRP3 inflammasome and MS/EAE. *Autoimmune Dis* 2013:859145.
27. Lin CC, Edelson BT (2017) New insights into the role of IL-1β in experimental autoimmune encephalomyelitis and multiple sclerosis. *J Immunol* 198:4553–4560.
28. Schuh E, et al. (2015) Expanding spectrum of neurologic manifestations in patients with NLRP3 low-penetrance mutations. *Neurol Neuroimmunol Neuroinflamm* 2:e109.
29. Kitley JL, Lachmann HJ, Pinto A, Ginsberg L (2010) Neurologic manifestations of the cryopyrin-associated periodic syndrome. *Neurology* 74:1267–1270.
30. Compeyrot-Lacassagne S, Tran TA, Guillaume-Czitrom S, Marie I, Koné-Paut I (2009) Brain multiple sclerosis-like lesions in a patient with Muckle-Wells syndrome. *Rheumatology (Oxford)* 48:1618–1619.
31. Shaw PJ, et al. (2010) Cutting edge: Critical role for PYCARD/ASC in the development of experimental autoimmune encephalomyelitis. *J Immunol* 184:4610–4614.
32. Gris D, et al. (2010) NLRP3 plays a critical role in the development of experimental autoimmune encephalomyelitis by mediating Th1 and Th17 responses. *J Immunol* 185:974–981.
33. Coll RC, et al. (2015) A small-molecule inhibitor of the NLRP3 inflammasome for the treatment of inflammatory diseases. *Nat Med* 21:248–255.
34. Matute C, et al. (2007) P2X(7) receptor blockade prevents ATP excitotoxicity in oligodendrocytes and ameliorates experimental autoimmune encephalomyelitis. *J Neurosci* 27:9525–9533.
35. Inoue M, et al. (2016) An interferon-β-resistant and NLRP3 inflammasome-independent subtype of EAE with neuronal damage. *Nat Neurosci* 19:1599–1609.
36. Inoue M, et al. (2012) Interferon-β therapy against EAE is effective only when development of the disease depends on the NLRP3 inflammasome. *Sci Signal* 5:ra38.
37. Martin BN, et al. (2016) T cell-intrinsic ASC critically promotes T(H)17-mediated experimental autoimmune encephalomyelitis. *Nat Immunol* 17:583–592.
38. Inoue M, Williams KL, Gunn MD, Shinohara ML (2012) NLRP3 inflammasome induces chemotactic immune cell migration to the CNS in experimental autoimmune encephalomyelitis. *Proc Natl Acad Sci USA* 109:10480–10485.
39. Dumas A, et al. (2014) The inflammasome pyrin contributes to pertussis toxin-induced IL-1β synthesis, neutrophil intravascular crawling and autoimmune encephalomyelitis. *PLoS Pathog* 10:e1004150.
40. Ming X, et al. (2002) Caspase-1 expression in multiple sclerosis plaques and cultured glial cells. *J Neurol Sci* 197:9–18.
41. Burm SM, et al. (2016) Expression of IL-1β in rhesus EAE and MS lesions is mainly induced in the CNS itself. *J Neuroinflammation* 13:138.
42. Dey A, Kang X, Qiu J, Du Y, Jiang J (2016) Anti-inflammatory small molecules to treat seizures and epilepsy: From bench to bedside. *Trends Pharmacol Sci* 37:463–484.
43. Mamik MK, et al. (2017) HIV-1 viral protein R activates NLRP3 inflammasome in microglia: Implications for HIV-1 associated neuroinflammation. *J Neuroimmune Pharmacol* 12:233–248.
44. Agresti C, et al. (2005) ATP regulates oligodendrocyte progenitor migration, proliferation, and differentiation: Involvement of metabotropic P2 receptors. *Brain Res Brain Res Rev* 48:157–165.
45. Selmaj KW, Raine CS (1988) Tumor necrosis factor mediates myelin and oligodendrocyte damage in vitro. *Ann Neurol* 23:339–346.
46. Ellestad KK, et al. (2009) Early life exposure to lipopolysaccharide suppresses experimental autoimmune encephalomyelitis by promoting tolerogenic dendritic cells and regulatory T cells. *J Immunol* 183:298–309.
47. Boghozian R, et al. (2017) Suppressed oligodendrocyte steroidogenesis in multiple sclerosis: Implications for regulation of neuroinflammation. *Glia* 65:1590–1606.
48. Hametner S, et al. (2013) Iron and neurodegeneration in the multiple sclerosis brain. *Ann Neurol* 74:848–861.
49. Prineas JW, Parratt JD (2012) Oligodendrocytes and the early multiple sclerosis lesion. *Ann Neurol* 72:18–31.
50. Ofengeim D, et al. (2015) Activation of necroptosis in multiple sclerosis. *Cell Rep* 10: 1836–1849.
51. Wen S, et al. (2017) Necroptosis is a key mediator of enterocytes loss in intestinal ischaemia/reperfusion injury. *J Cell Mol Med* 21:432–443.
52. Miao EA, Rajan JV, Aderem A (2011) Caspase-1-induced pyroptotic cell death. *Immunol Rev* 243:206–214.
53. Wang Y, et al. (2017) Chemotherapy drugs induce pyroptosis through caspase-3 cleavage of a gasdermin. *Nature* 547:99–103.
54. Ben-Sasson SZ, et al. (2013) IL-1 enhances expansion, effector function, tissue localization, and memory response of antigen-specific CD8 T cells. *J Exp Med* 210:491–502.
55. Thornton P, Pinteaux E, Gibson RM, Allan SM, Rothwell NJ (2006) Interleukin-1-induced neurotoxicity is mediated by glia and requires caspase activation and free radical release. *J Neurochem* 98:258–266.
56. Takahashi JL, Giuliani F, Power C, Imai Y, Yong VW (2003) Interleukin-1beta promotes oligodendrocyte death through glutamate excitotoxicity. *Ann Neurol* 53:588–595.
57. Vertex Pharmaceuticals Incorporated (2007) Phase 2 clinical study in psoriasis with oral investigational drug VX-765. Clinical trial. Available at https://clinicaltrials.gov/ct2/show/NCT00205465?id=NCT00205465&rank=1. Accessed May 22, 2018.
58. Vertex Pharmaceuticals Incorporated (2010) Study of VX-765 in subjects with treatment-resistant partial epilepsy. Clinical trial. Available at https://clinicaltrials.gov/ct2/show/NCT01048255?id=NCT01048255&rank=1. Accessed May 22, 2018.
59. Bassil F, et al. (2016) Reducing C-terminal truncation mitigates synucleinopathy and neurodegeneration in a transgenic model of multiple system atrophy. *Proc Natl Acad Sci USA* 113:9593–9598.
60. Ronchi F, et al. (2016) Experimental priming of encephalitogenic Th1/Th17 cells requires pertussis toxin-driven IL-1β production by myeloid cells. *Nat Commun* 7:11541.
61. Lukens JR, Barr MJ, Chaplin DD, Chi H, Kanneganti TD (2012) Inflammasome-derived IL-1β regulates the production of GM-CSF by CD4(+) T cells and γδ T cells. *J Immunol* 188:3107–3115.
62. Dungan LS, Mills KH (2011) Caspase-1-processed IL-1 family cytokines play a vital role in driving innate IL-17. *Cytokine* 56:126–132.
63. Mamik MK, et al. (2016) Insulin treatment prevents neuroinflammation and neuronal injury with restored neurobehavioral function in models of HIV/AIDS neurodegeneration. *J Neurosci* 36:10683–10695.
64. Monaco MC, et al. (2012) Progenitor-derived oligodendrocyte culture system from human fetal brain. *J Vis Exp*, 10.3791/4274.
65. Walsh JG, et al. (2014) Rapid inflammasome activation in microglia contributes to brain disease in HIV/AIDS. *Retrovirology* 11:35.
66. Goncalves DaSilva A, Yong VW (2009) Matrix metalloproteinase-12 deficiency worsens relapsing-remitting experimental autoimmune encephalomyelitis in association with cytokine and chemokine dysregulation. *Am J Pathol* 174:898–909.
67. Schindelin J, et al. (2012) Fiji: An open-source platform for biological-image analysis. *Nat Methods* 9:676–682.